PERGAMON

Journal of Structural Geology 22 (2000) 1723–1735

JOURNAL OF STRUCTURAL GEOLOGY

www.elsevier.nl/locate/jstrugeo

Mollusc shell microstructures and crystallographic textures

D. Chateigner[a,*], C. Hedegaard[b], H.-R. Wenk[c]

[a]*Laboratoire de Physique de l'Etat Condensé, Université Du Maine, Le Mans, France*
[b]*Institute of Biology, Department of Ecology and Genetics, University of Aarhus, Aarhus, Denmark*
[c]*Department of Geology and Geophysics, University of California, Berkeley, CA, USA*

Received 30 November 1999; accepted 26 June 2000

Abstract

X-ray diffraction is used to characterise textures of the aragonite layers of shells from monoplacophoras, bivalves, cephalopods and gastropods. Textures vary in strength, pattern and through the thickness of the shells. The texture patterns exhibited in the studied taxa, which can be quantitatively described by a limited number of parameters, are compared with the microstructure types observed with scanning electron microscopy. Whereas for simple crystallite arrangements, such as nacres, there is a good correspondence between texture and microstructure, this is often not the case in more complex microstructures such as in crossed lamellar layers. Morphologically similar microstructures may have different crystallographic textures, and the same textures may be found in microstructures with different morphology. These two kinds of measurements are shown to be complementary since they provide non-redundant information for many taxa, which suggests that they may be valuable phylogenetic indicators.

1. Introduction

The investigation of mollusc shell microstructures, built of complex calcite and/or aragonite layer intergrowths, is of interest in many fields of science. In geology, since shells are the most commonly preserved parts in fossils, they are used to determine the phylogenetic evolution and specify the stratigraphic age of geological formations. Palaeontology has largely relied on scanning electron microscopy for a precise description of shell microstructures (Taylor et al., 1973; Carter, 1980; Carter and Clark, 1985; Hedegaard, 1990; Hedegaard, 1997). Nacre is significant in medicine. Maya Indians of Honduras already used nacre for dental implants 2000 years ago (Bobbio, 1972). In modern orthopaedic medicine, aragonite of *Pinctada maxima* stimulates bone growth by human osteoblasts (Silve et al. 1992). Natural processes driving biomineralisation of calcium carbonate are still enigmatic, though much progress has been made, linking shell formation to protein substrates and templates (Crick, 1989; Suga and Nakahara, 1991; Weiner and Traub, 1984).

Microstructural properties of mollusc shells were investigated extensively by means of thin sections (Bøggild, 1930). Among the microstructural characteristics, the orientation distribution of crystallographic axes (texture) dominates the anisotropic properties of aggregates (Kocks et al., 1998). However, only few papers consider the aggregate properties of shells (Bøggild, 1930; Wenk, 1965; Wilmot et al., 1992). Mutvei (1978, 1980) hypothesised about the crystallographic properties of nacre tablets, but his conclusions have been at least partly refuted by recent investigations (Hedegaard and Wenk, 1998).

In order to use the microstructural information in phylogeny, one has to explore if all the components of the microstructure (crystallographic textures and grain morphology, grain sizes and boundaries) are not redundant. We investigate the relationship between texture and the morphological elements (as seen with a scanning electron microscope (SEM)) of mollusc shell microstructures. Two questions that arise are:

1. whether the microstructural elements are'simple crystals', that is whether textures reflect the geometry of the structural elements;
2. whether there is a one-to-one relationship between textures and microstructures and a given microstructure always has a specific texture pattern, or if a given texture pattern only occurs in one microstructure type.

This work is part of an on-going systematic analysis of mollusc shell textures to build a new character set for phylogenetic analysis, equally applicable to extant and fossil taxa.

* Corresponding author.
E-mail address: daniel.chateigner@univ-lemans.fr (D. Chateigner).

0191-8141/00/$ - see front matter
PII: S0191-8141(00)00088-2

2. Material

We examined nearly 50 species as representatives of the taxa (Table 1), with up to four different layers being explored for some species. We sampled most of the major molluscan clades and several taxa with each of the main shell structures (Bøggild, 1930; Taylor, et al., 1969, 1973; Hedegaard, 1990). For technical reasons, sampling is skewed towards larger individuals. Samples for texture analysis need to be close to planar, and should comprise a small portion of the investigated shell. Curved or uneven samples cause defocusing of the X-rays and uncontrolled absorption of the beam. Samples of approximately 1 cm in diameter do not cause geometrical effects and generally allow quantitative results. Mostly we had to investigate smaller samples, as small as approximately 5 mm in diameter.

3. Texture and microstructure analyses

For all analyses, the principal directions within the shells were first defined with an optical microscope. We decided to use the following macroscopic sample reference frame for texture and SEM descriptions:

1. the growth direction, **G**, perpendicular to the margin of the shell (Fig. 1a) is the vertical axis of our pole figures (Fig. 1b), and the horizontal axis of the SEM images, unless specified in the caption;
2. the plane tangent to the shell, defined by the sample holder plane, has its normal, **N**, as the normal axis in the centre of the pole figures and the vertical axis of the SEM images;
3. the third axis, **M**, direction of the growth lines of the outside layer, is horizontal in the pole figures.

Discussions refer to the orthorhombic mineral aragonite that composes most mollusc layers. We have also investigated textures of a few calcite layers but they will not be discussed in this paper.

3.1. Microstructures

We examined shell microstructures of fractured specimens with either an Electroscan Environmental SEM at the University of California (Berkeley), Museum of Palaeontology, that does not require specimens to be metal coated; or with a standard SEM HITACHI S2300 instrument at the Université du Maine (Le Mans). Specimens were mounted on aluminium stubs with double-sticky tape (small specimens) or plaster of Paris. The shell layer microstructure was determined and described by the terminology of the following section, using a low magnification microscope. This helped us also in determining areas of interest (typically of several millimeters squared) for the following X-ray analysis.

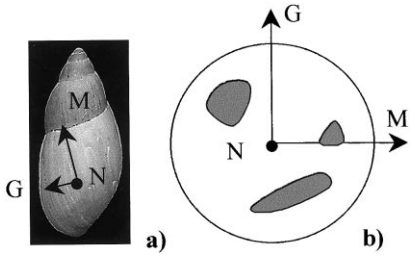

Fig. 1. Example for the definition of the macroscopic sample reference frame on a *Euglandina sp.* (a), and corresponding pole figure axes (b).

We generally measured the inner and outer layers of specimens. It is difficult to sample the intermediate layers of a shell. They must be exposed by grinding and etching in a surface of several millimeters on each side, and also be thick enough to leave a sufficiently thick layer (minimum 0.1 mm, in respect of the penetration of X-rays in these materials) for texture analysis. Consequently, we only have sparse data for intermediate layers, but abundant data for interior and exterior layers.

3.2. X-ray texture analysis

We used X-ray diffraction to determine the orientation distribution of thousands of crystallites in area 1–3 mm in diameter, relative to the macroscopic frame defined by **G**, **N** and **M** (Fig. 1). Inner and outer layers of specimens must be thick enough (≥ 0.1 mm) in order not to receive diffracted signals from the deeper layers.

Over 3 years of investigations, we used two X-ray diffractometers equipped with four-circle goniometers, and monochromatic radiations. The first instrument, at U.C. Berkeley, uses a point detector and Fe Kα radiation, with wide receiving slits (Chateigner et al., 1996). The second diffractometer, at Le Mans, uses the INEL-CPS120 curved position sensitive detector and Cu Kα radiation, which records the whole diffraction diagram simultaneously. Both instruments give reliable and reproducible results (Ricote and Chateigner, 1999; Ricote et al., 2000). Once the pole figure data are corrected for defocusing, absorption, volume and sample distortion (Heizmann and Laruelle, 1986), the quantitative texture analysis was made with the Berkeley Texture Package (Wenk et al., 1998). When a good reproducibility of the experimental pole figures and satisfying reliability factors were obtained, the orientation distribution was used to recalculate the {001} and {100} pole figures. Typical results for data reliability were discussed previously (Chateigner et al., 1996). Fig. 2 shows a typical X-ray diffraction pattern as obtained with the position sensitive detector, for the aragonite nacre layer of *Mytilus edulis*. It represents the sum of all the 936 experimental diagrams measured for every position of the sample. We can index up to nine different reflections or groups of reflections of the aragonite and those can be used for the quantitative texture analysis. Note that sample geometry is often a major obstacle. We have found data to be highly reproducible, but shells are invariably curved and uneven, causing defocusing, absorption

Table 1
Results of the texture investigations of all samples investigated: V_T is the normalised twinned volume fraction, $\{001\}_{max}$ the maximum {001} pole density, and F^2 the texture index (a '–' means that data could not be refined by QTA). ICN: inside columnar nacre; ISN: Inside Sheet Nacre; ICL: Inside Comarginal Crossed Lamellar; ICCL: Inner Complex Crossed Lamellar; IICCL: Inner Irregular Complex Crossed Lamellar; IRCL: Inner Radial Crossed Lamellar; ISP: Inner Simple Prismatic. OCL: Outer Comarginal crossed Lamellar; OFSP: Outer Fibrous Simple Prismatic; ORCL: Outer Radial Crossed Lamellar; OSP: Outer Simple Prismatic; OSpP: Outer Spherulitic Prismatic; OH: Outer Homogeneous; OICP: Outer Intersected Crossed Platy

Taxon	Layer microstructure	c-axis	a-axis	Direction from G	V_T (%)	$\{001\}_{max}$ (m.r.d.)	F^2 (m.r.d.^{2})
Bivalves							
Acila castrensis	ISN	⊥	*	<100>, 90	-	63	88
Anodonta cygnea	ISN	⊥	*	<100>,125	38	49	49
	OFSP	⊥	O	-	-	18	7.1
Atrina maurea	ISN	⊥	*	<100>, 160	67	>100	241
Bathymodiolus thermophilus	ISN	⊥	*	<100>, 90	57	84	65
Fragum fragum	ICL	∀, 15	×	<110>	100	49	46
Glycymeris gigantea	ICL	∀, 15	×	<110>	100	35	55
Lampsilis alatus	ISN	⊥	*	<100>, 90	38	>100	175
Mytilus californianus	ISN	⊥	*	<100>, 90	65	25	77
Mytilus edulis	ISN	⊥	*	<100>, 90	52	>100	51
Neotrigonia sp.	ISN	⊥	*	<100>, 90	18	>100	210
Pinctada margaritifera	ISN	⊥	*	<100>, 90	12	>100	>9999
Pinctada maxima	ISN	⊥	*	<100>, 90	21	>100	746
Pinna nobilis	ISN	⊥	*	<100>, 95	38	>100	>9999
Pteria penguin	ISN	⊥	*	<100>, 120	23	>100	429
Spondylus princeps	RCL	⊥	O	-	-	>100	164
	ICL	∨, 10	×	<110>, 105	100	37	47
Sunetta solanderii	ICL	⊥	O	-	-	>100	177
	OFSP	∠, 20	O	-	-	40	44
Tapes japonica	IRCL	⊥	O	-	-	>100	130
Cephalopods							
Nautilus macromphalus	ICN	⊥	*	<100>, 100	50	>100	333
	OH	⊥	*	<100>, 75	50	65	16
Nautilus pompilius	ICN	⊥	*	<100>, 75	92	51	51
Gastropods							
Cellana testudinaria	IICCL	⊥	×	<100>, 120	-	-	-
Conus leopardus	ICL	⊥	×	<100>, 30	94	52	201
	ORCL	⊥	O	-	-	5	29
Cyclophorus woodianus	IRCL	⊥	|	<100>, 20	0	>100	297
	ORCL	⊥	O	-	-	-	-
Cypraea mus	ISP	⊥	*	<100>, 45	-	-	-
	RCL	⊥	×	<100>, 60	-	-	-
	OCL	⊥	×	<100>, 105	92	63	118
Cypraea testudinaria	ICL	∨, 15	|	<100>, 10	-	>100	432
	RCL	∀, 25	×	<110>, 75	92	28	32
	CL	⊥	*	<100>, 90	-	28	41
	OH	∀, 15	*	<100>, 90	26	55	78
Entemnotrochus adansonianus	ISP	⊥	O	-	-	-	-
	CN	⊥	O	-	-	-	-
	OICP	⊥	O	-	-	-	-

Table 1 (*continued*)

Euglandina sp.	IRCL	⊥	|	<100>, 80	0	>100	307
	OCL	⊥	|	<100>, 120	0	23	40
Fissurella oriens	IICCL	⩒, 20	*	<110>	83	33	76
Haliotis cracherodi	ICN	∠, 15	O	-	-	>100	90
Haliotis rufescens	ICN	⊥	O	-	-	-	-
Helix aspersa (A)	OCL	⊥	|	<100>, 90	0	38	80
(B)	OCL	⊥	|	<100>, 90	0	42	92
Helix pomatia	OCL	⊥	|	<100>, 90	0	55	105
Helminthoglypta nickliniana anachoreta	OCL	⊥	*	<100>, 90	18	45	103
Muricanthus nigritus	ICL	⊥	×	<100>, 140	94	86	119
	OCL	⊥	×	<100>, 125	98	32	46
Nerita polita	ICL	∠, 25	*	<100>	88	29	27
Nerita scabricosta	IICCL	⊥	O	-	-	34	26
Oliva miniacea	OCL	⊥	×	<100>, 30	100	45	103
	OH	⊥	*	<100>, 115	17	>100	526
Perotrochus quoyanus	ICN	⊥	O	-	-	-	-
	OICP	⊥	O	-	-	-	-
Phasianella australis	CL	⊥	O	-	-	18	8.7
	OICP	⊥	O	-	-	-	-
Scutellaster tabularis	IRCL	⩒, 25	×	<110>, 100	100	42	76
Scutus antipodes	CL	⩒, 15	×	<110>, 5	27	23	34
	ICCL	⊥	*	<100>, 30	88	23	18
Tectus niloticus	ICN	⊥	O	-	-	>100	88
	OSpP	∠, 15	O	-	-	-	-
Tectus pyramis	OSpP	∠, 15	O	-	-	62	26
Turbo petholatus	OICP	⊥	O	-	-	26	17
Viana regina	IICCL	⊥	O	-	-	64	68
	OCL	⊥	O	-	-	18	10
Monoplacophoras							
Neopilina galatheae	ISN	⊥	O	-	-	-	-
	OSP	⊥	O	-	-	-	-
Rokopella zographi	ISN	⊥	O	-	-	-	-

and volume variations. Consequently, in some instances we had to omit data within a sample. Using the point detector we used the {111}, {021}, {102/200}, {121/012} and {221} pole figures, while making use of the PSD allowed to also use the {002}, {112/022/031/130}, {041/202} and {113/141/231/023} groups.

A measure of the texture strength is given for samples with satisfactory reliability. It is given as bulk 'texture index', or F^2 (Bunge, 1981), and as the maximum pole density of the {001} pole figure. The former gives an overall measure of the strength, while the latter is only related to the dispersion of the *c*-axes. Both criteria increase with the strength of the texture. We estimate that measurements and calculations are reliable within 10%. We performed experiments on different locations of a curved shell surface of *Helix aspersa* (Fig. 3). The texture calculations provide a texture index of 80 m.r.d.^{2} and 92 m.r.d.^{2}, and a maximum density of the {001} pole figure of 42 m.r.d. and 38 m.r.d., illustrated in Fig. 3 (a) and (b) respectively.

4. Microstructures observed with the SEM

The terminology of shell microstructures is usually based on the morphology of sub-units as observed in thin-sections with a petrographic microscope or with an SEM. We

describe shell microstructures using the terminology of Carter and Clark (1985), but emphasise that these definitions only represent a terminology (the names are convenient, brief summaries of observed morphologies), not necessarily a statement of homology. We use 'first-order' and 'second-order' (prisms, lamellae), to describe increasingly fine microstructural elements with morphological distinction. For instance, simple crossed lamellar structure is composed of 'first-order lamellae' (approx. 10 μm thick), each of which is composed of 'second-order lamellae' (1 μm in thickness).

4.1. Prismatic microstructures

Shell layers with "mutually parallel, adjacent structural units (first-order prisms) that do not strongly interdigitate along their mutual boundaries" (Carter and Clark, 1985, p. 52) are simple prismatic (SP, Fig. 4a). Simple prismatic microstructures may be composed of either aragonite or calcite.

Spherulitic prismatic microstructure (SpP) has coarse first order prisms, with second-order prisms originating in spherulitic sectors at the depositional surface (Fig. 4b). They appear as fans of radial laths in vertical sections. This microstructure is invariably in our material composed of aragonite.

4.2. Nacreous microstructures

Nacreous microstructures are "aragonitic laminar structures consisting of polygonal to rounded tablets arranged in broad, regularly formed, parallel sheets" (Carter and Clark, 1985, p. 55). Nacres are 'columnar nacre' (CN) or 'sheet nacre' (SN) depending on the stacking mode of the tablets. Columnar nacre (Fig. 5a) has tablets of rather uniform size with coinciding centres, that determine the nucleation site of the overlying tablet (Mutvei, 1980). In sheet nacre (Fig. 5b), deposition takes place over most of the inner surface of the shell, and the tablets are stacked in a 'brick wall' pattern, spanning the interface between underlying tablets.

4.3. Crossed microstructures

Simple crossed lamellar microstructures (CL, Fig. 6a) have first-order lamellae of thin, mutually parallel laths or rods, with two non-horizontal dip directions of their elongate sub-units in adjacent lamellae. The structure is comarginal, if the first-order lamellae are parallel to the shell margin, radial if perpendicular. This kind of microstructure is widely distributed among molluscs (MacClintock, 1967; Taylor et al., 1969, 1973; Runnegar et al., 1975; Lindberg, 1988; Carter, 1990; Hedegaard, 1990, 1997).

Complex crossed lamellar microstructures (CCL, Fig. 7a) have first-order lamellae with more than two dip directions. The "first order lamellae consisting of irregularly shaped, interpenetrating aggregations of parallel second order structural units" (Carter and Clark, 1985) appear as an aggregate of intergrown pieces of simple crossed lamellar structure.

Intersected crossed platy microstructure (ICP, Fig. 7b) is "a crossed structure with two predominant dip directions consisting of intersected platy crystallites" (Carter and Clark, 1985, p. 62). This microstructure only occurs in some vetigastropods (Hedegaard, 1990), and is identical to the "Type II crossed lamellar structure" of Batten (1975).

4.4. Homogeneous

Homogeneous microstructure (H, Fig. 8) is an unfortunate name, implying no discernible substructure. Bøggild (1930, p. 245) described it from thin-sections, as "in ordinary light we see…no structure at all", but pointed out it has an arrangement of the crystallographic axes. Carter and Clark

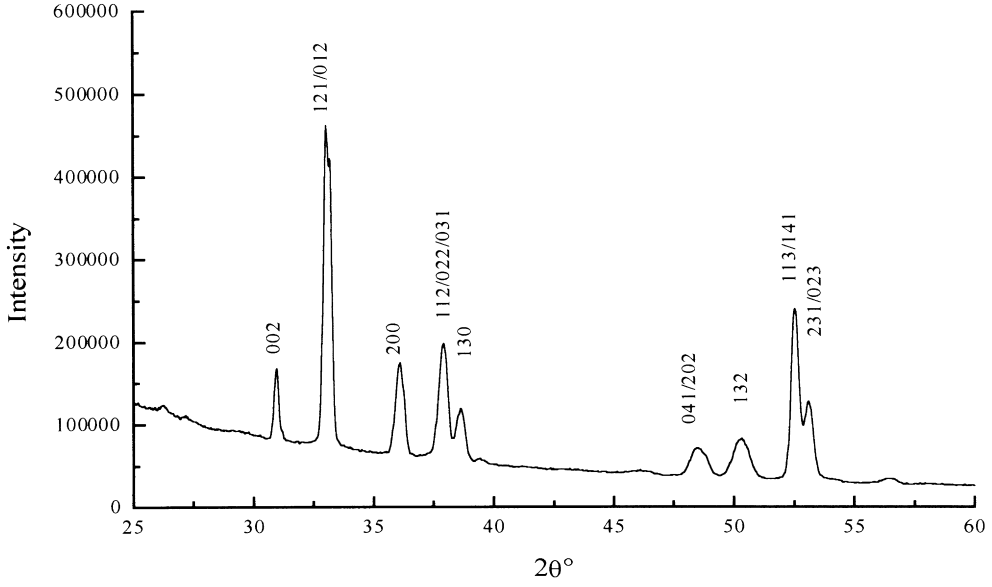

Fig. 2. Typical X-ray diffraction pattern obtained with the curved detector for the nacre layer of *Mytilus edulis*, showing the experimental resolution and the reflections accessible for quantitative texture analysis.

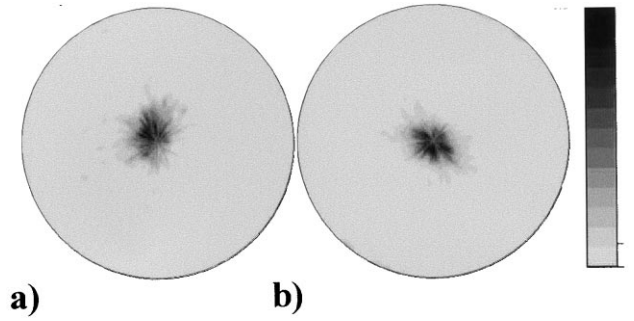

Fig. 3. {001} Pole figures of two specimens of *Helix aspersa* showing the reliability of the texture analysis: (a) specimen A (max = 42 m.r.d.); (b) Specimen B (max = 38 m.r.d.). Logarithmic density scale, equal area projection.

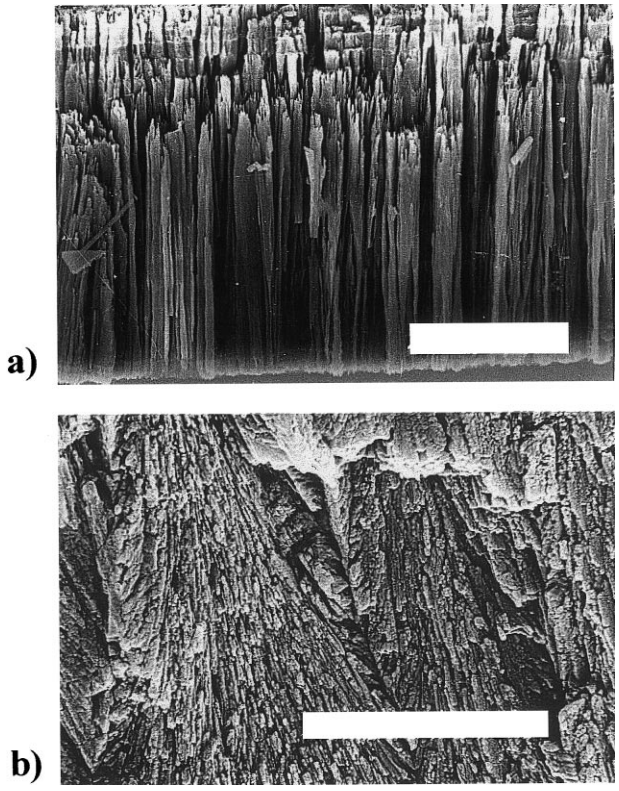

Fig. 4. SEM image of prismatic microstructures: (a) regular simple prismatic of the innermost layer of *Turbo petholatus* (scale bar = 15μm); (b) irregular spherulitic prismatic layer of *Tectus conus* (scale bar = 20 μm).

(1985, p. 63) describe it as "aggregations of more or less equidimensional, irregularly shaped crystallites lacking clear first-order structural arrangement except for possible accretion banding". In other words, when a shell structure has no other identifiable elements than minute granules, it is homogeneous.

5. Texture patterns

Fig. 9 summarises the texture patterns that have been

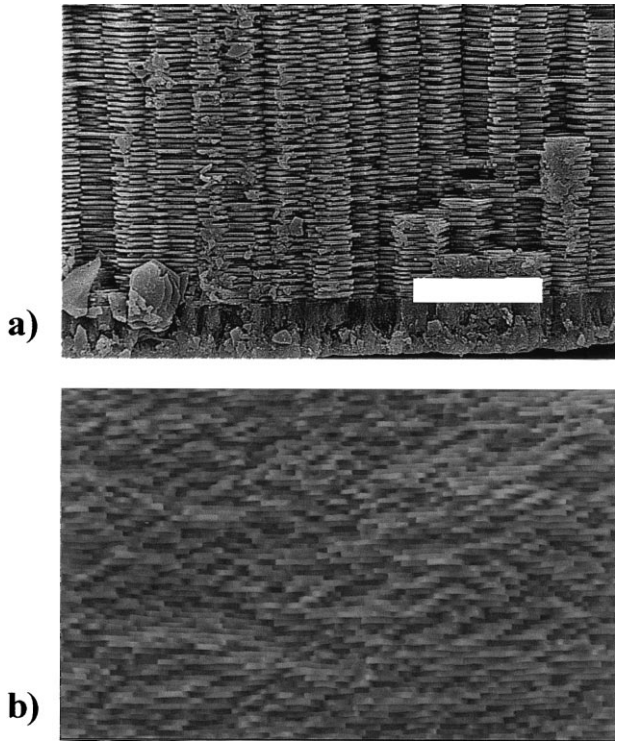

Fig. 5. SEM image of nacreous microstructures: (a) columnar nacre of *Turbo undulatus* (scale bar = 20 μm); (b) sheet nacre of *Pinctada margaritifera* (scale bar = 40 μm). The *c*-axes are orthogonal to the hexagonal platelets.

observed in {001} and {100} pole figures. Table 1 presents the qualitative and quantitative results of the texture analysis for all the analysed taxa and the shell structures of the analysed layers. In this table, a '–' in the F^2 column means that quantitative texture analysis (QTA) was not possible from the acquired data, usually because the geometry of the shell was not regular enough to ensure a constant X-ray irradiated surface. In fibre textures, a '–' for 'twinned volume fraction' indicates that this parameter cannot be found by QTA for this texture type, and for 'direction // **G**' that all directions of the (a, b) planes have an equal probability to be aligned with **G**. When the texture strength equals or exceeds the maxima imposed by the software, we enter >100 and >9999 in Table 1 to indicate that the maximum pole density of the {001} pole figure and the texture index are larger than 100 m.r.d. and 9999 m.r.d.^{2}, respectively.

Previously, noting that characteristic texture patterns exist in most shells, we found it useful to develop a systematic terminology (Chateigner et al., 1999). Fig. 9 gives examples of the distributions of *c*- and *a*-axes (left and right column respectively), and their corresponding symbols. For **c** axes, ⊥ symbolises a *c*-axis texture maximum with a centre aligned with **N** (Fig. 9a), whereas ∠ means that the maximum has an angle α with **N** (Fig. 9b). If the *c*-axis maximum is dispersed by an angle α at half maximum, the representation is $\underline{\forall}$ (Fig. 9c), while $\underline{\perp}$ indicates

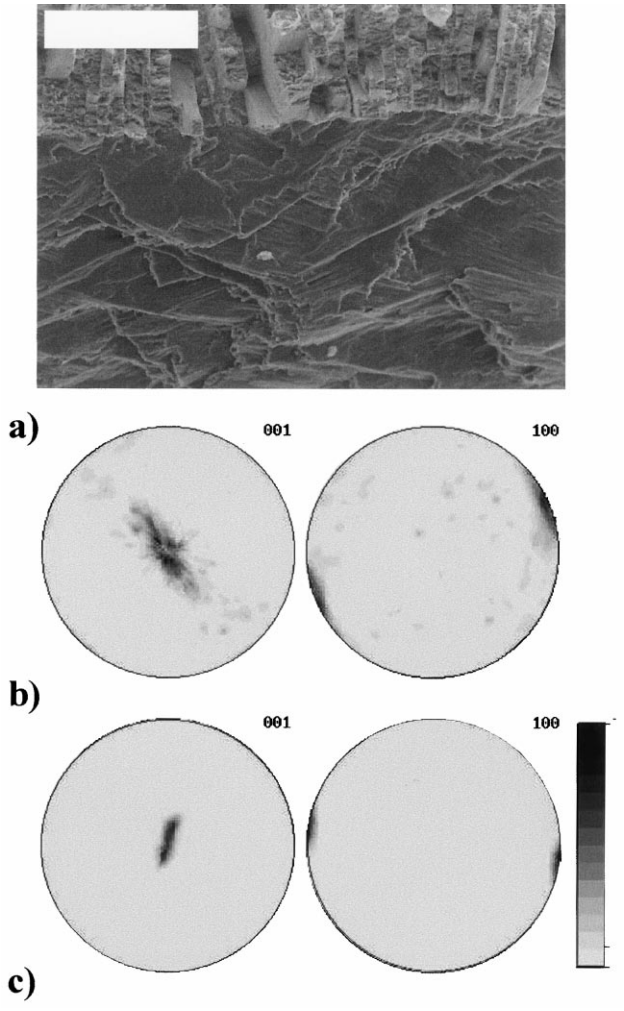

Fig. 6. (a) SEM backscattering image of the interface of *Euglandina sp.* (scale bar = 100 μm). The outer comarginal crossed lamellar layer (OCL) is on top of the image, the inner radial crossed lamellar layer at bottom (IRCL). Note the well-defined crossed microstructure. (b) {100} and {001} Pole figures of the OCL (max = 23 m.r.d., min = 0). (c) {100} And {001} pole figures of the IRCL (max >100 m.r.d., min = 0). Note the single crystal texture pattern. Linear density scale, equal area projection.

a split of the component with an angle α between the two individuals (Fig. 9d).

For the *a*-axis distribution, we use the | symbol for a single crystal-like pattern (Fig. 9e), and an angle β gives the location of the *a*-axes relative to **G**. If the {100} pole figure exhibits four maxima (two orientation components), a × (Fig. 9f) is used, while a * is assigned for six maxima (three components, Fig. 9g). These latter features are referred to as single or double twinning (on {110} planes) respectively. However, X-ray texture analysis probes several thousands of cristallites, and we can not distinguish if individual crystallites are intrinsically twinned or if the observed pole figures result from a regular stacking of single crystals. A more local investigation, e.g. transmission electron microscopy would be needed to prove that twinning actually occurs in individual crystallites of aragonite (Wilmot et al., 1992). Finally, a perfectly random

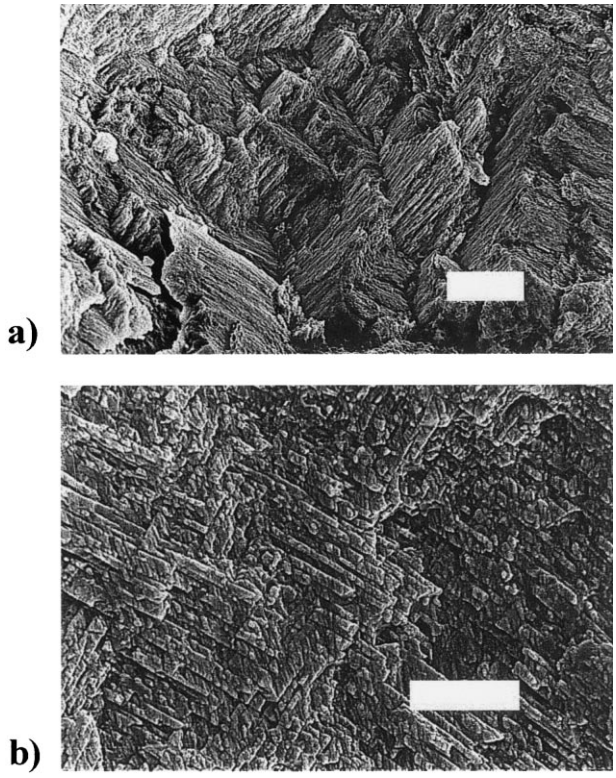

Fig. 7. SEM image of (a) irregular complex crossed lamellar layer of *Fissurellidea aperta* (scale bar = 20 μm), horizontal axis is **M**, and (b) intersected crossed platy layer of *Liota granulosa* (scale bar = 5 μm), horizontal axis is **G**.

distribution of the *a*-axes around *c* (fibre texture) is indicated by ○ (Fig. 9h).

When twin-like patterns are observed, it is possible to estimate the relative volume fractions associated to each of the components of the twin, taking the density ratios of the components in {100} pole figures. For instance, if the sample is entirely twinned, a double twin pattern has three orientations and a third of the total volume will be in each orientation, corresponding to three equally strong intensities in the {100} pole figure. Frequently we observe one orientation is considerably stronger than the others, and we calculate the

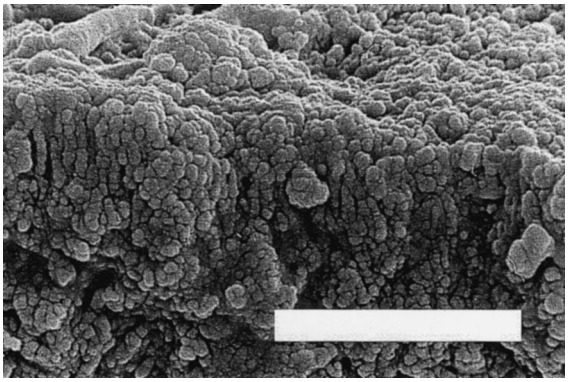

Fig. 8. SEM image of the homogeneous outermost layer of *Liota granulosa* (scale bar = 5 μm), horizontal axis is **M**.

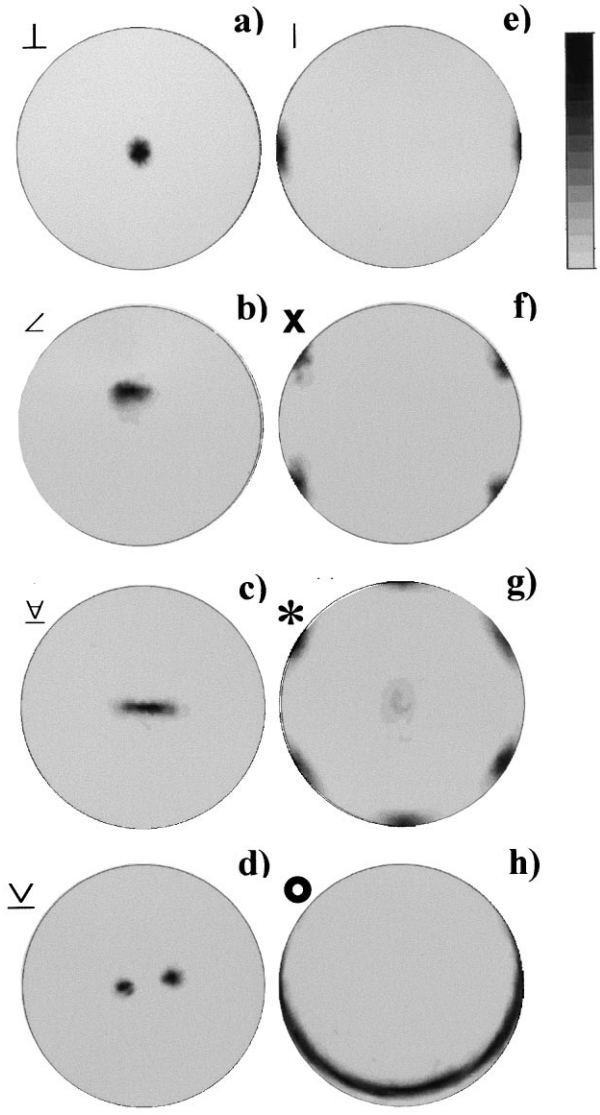

Fig. 9. Recalculated {001} and {100} pole figures (left and right columns respectively) for typical texture patterns: (a) perpendicular (*Pinctada maxima,* maximum density > 100 m.r.d.); (b) tilted (*Nerita polita* max: 29 m.r.d.); (c) dispersed (*Fragum fragum* max: 35 m.r.d.); (d) split (*Cypraea testudinaria* max > 100 m.r.d.); (e) single-crystal like (*Helix pomatia* max: 55 m.r.d.); (f) single twin (*Conus leopardus* max: 49 m.r.d.); (g) double twin (*Nautilus pompilius* max: 23 m.r.d.); (h) fibre (*Haliotis cracherodi* max: 12 m.r.d.). Linear density scale, equal area projection. Minimum densities are zero.

normalised percentage of twinned fraction, using the maximum densities of the recalculated {100} poles. This is the ratio between the sum of the two weakest components to the total density, normalised to 66.67% (double twin patterns) or 50% (single twin patterns). As an example, a fully double twinned sample will have a third of the intensity in each of three orientations and have a normalised twinned volume fraction of 100% (close to the case of *Muricanthus nigritus,* Table 1). Similarly, a fully single twinned sample has 50% of the reflections from each of the two orientations, and the normalised twinned volume fraction is 100% (case of *Fragum fragum*). This measure allows us to easily compare the amount of twinned material across samples with different textures.

Table 2
Distribution of the microstructural types observed versus main features of the texture patterns. SP: Simple prismatic; SpP: Spherulitic prismatic; CN: columnar nacre; SN: sheet nacre; CL: comarginal crossed lamellar; RCL: radial crossed lamellar; ICCL: irregular complex crossed lamellar; ICP: intersected crossed platy; H: homogeneous

	⊥	⩒	∠	∀	|	x	*	O
SP	+		+				+	+
SpP			+					+
CN	+		+				+	+
SN	+						+	+
CL	+	+	+	+	+	+	+	+
RCL	+	+		+	+	+		+
ICCL	+	+				+	+	+
ICP	+							+
H	+			+			+	

Mollusc shells have very strong textures; the nacre tablets of *Pinctada maxima* are perfectly aligned, and large domains of the shell show a common alignment of axes, resembling a single-crystal or textures observed in epitaxial films. Only an insignificant portion of crystallites is randomly oriented. *Pinctada maxima* is an extreme case, but all the samples investigated exhibit minimal volume fractions of randomly oriented crystallites. As mentioned above, the strength of the observed textures reaches in some cases extreme values (e.g. *Pinctada margaritifera*). However, even for such a high texture strength, our calculations indicate a full texture peak width at half maximum in the *c*-axis distribution of less than 5°, which is consistent with the angular dispersions observed by Weiner and Traub (1981) in *Pinctada radiata.*

It is difficult to compare our results with data from the literature. We were only able to find some diffraction studies, generally performed on thin sections. Wise (1970) and Weiner and Traub (1981), described the nacre layer of *Tectus dentatus* with a random distribution of *a*- and *b*-axes around *c*, which is the same as we observe in the closely related specimen of *Tectus niloticus*. Weiner and Traub (1981) observed strong three dimensional textures in the nacres of *Nautilus repertus, Pinctada radiata* and *Neotrigonia margariticea*, as our *Nautilus, Pinctada* and *Neotrigonia* specimens with twinned textures. The authors also mention a poor in-plane alignment of *Mytilus californianus* for which we observe a double twin texture, but with a comparatively low texture strength.

6. Discussion

Table 2 summarises the relationship between shell microstructural elements and texture patterns. This is not a

quantitative statistical study, because the number of examined taxa is small, and our data merely show the span of data. However, one can see that *c*-axes are mostly aligned parallel to the **N** direction (without splitting or dispersion), irrespective of the layers in the microstructure. When a split or a dispersion appears in the *c*-axis pattern, the average still remains aligned with **N**. Splitting and dispersions are common in crossed lamellar microstructures, while inclined *c*-axes are found in nacre or in prismatic microstructures. Also, the *a*-axis distributions appear more often as fibre textures than single crystal-like, with intermediate occurrences for double and single twinned layers. While none of the analysed shells shows random texture, the comarginal crossed lamellar layers exhibit the largest diversity in textural pattern. Both, intersected crossed platy and spherulitic prismatic layers, are characterised by a unique texture type, while complex crossed lamellar layers only show perpendicular *c*-axes. The *a*-axis distribution of nacre is more diverse for columnar than for sheet layers, while the opposite tendency is observed for the *c*-axes diversity.

The taxa where we sampled several layers (*Anodonta cygnea*, *Conus leopardus*, *Muricanthus nigritus*, *Nautilus macromphalus*, *Scutus antipodes*, *Sunetta solanderii*, *Viana regina*, but not *Spondylus princeps*, *Cypraea testudinaria* and *Oliva miniacea*) usually have stronger textures (larger F^2 value) on the inside than on the outside of the shell. This could result from epitaxial-like relationships between crystalline and/or organic layers and environmental effects.

Environmental effects are beyond the scope of this study since we would need data on textures for various development stages of a species. Texture analysis provides some information about the nature of shell growth. If the epitaxial-like texture increase was coming from purely crystalline interactions, one would expect a continuation of the microstructure type with a better alignment to a common frame. This is obviously not the case for *Anodonta cygnea*, *Cypraea testudinaria* and *Nautilus macromphalus*. At least in these species, the amount of organisation of layers increases even if layer microstructures are different, i.e. without common crystal lattice for epitaxy. Our diffraction technique provides no information on organic materials such as polypeptides, chitins and proteins which are related to preferred growth of calcium carbonate. This relationship has been investigated by Weiner and Traub (1980, 1981) and Weiner et al. (1983) for *Nautilus repertus*, using both X-ray and electron diffraction. These materials could be equally responsible for texture strength as they are for texture pattern, e.g. systematic changes through the thickness of the shells. This hypothesis is consistent with the observation that 'late layers', deposited on the outside of the adult shell by some species (*Oliva miniacea*, *Cypraea testudinaria*), have a larger texture strength than the younger inside layers. The glycoprotein control of growth has been studied in synthetic aragonite and calcite (Falini et al., 1996), in calcitic sponge spicules, and biogenic calcite crystals (Aizenberg et al., 1996; Aizenberg et al., 1997; Weiner and Addadi, 1997).

We observe single twinned layers in several crossed lamellar layers. This signifies that the organisms can differentiate between symmetry-related directions of the aragonite, and discriminate one member of the family. Aizenberg et al. (1996) observed a similar behaviour in calcitic sponge spicules in individual crystals. This is to our knowledge the first time that it is observed for aragonite at the macroscopic scale. The "anisotropic environment for crystal growing" invoked by Aizenberg et al. (1996) could then be responsible for the resulting single-twinned textures.

The simple prismatic structure of *Entemnotrochus adansonianus* (Table 1) has a fibre texture and the *c*-axis perpendicular to the shell layer. The *c*-axis is parallel to the maximum dimensions of the prisms, but the *a*- and *b*-axes of the individual prisms are not aligned relative to each other. The simple prismatic structure of *Cypraea mus* has a double twin texture and the *c*-axis is perpendicular to the shell layer, i.e. all the *a*- and *b*-axes of the individual prisms are in a well-defined orientation relationship. This demonstrates that morphologically similar layers with a similar position in the shell (on the inside) can have different textures.

Our samples with spherulitic prismatic microstructure originate from putatively closely related taxa and have fibre texture with the *c*-axis inclined relative to the shell surface. This texture occurs in other microstructures of additional taxa (columnar nacre of *Haliotis cracherodi*, fibrous simple prismatic layer of *Sunetta solanderii*) in a larger clades, and is thus not restricted to spherulitic prismatic microstructures. If each of the individual needles of the spherulitic prismatic microstructures were crystallographically identical (e.g., crystallographic *c*-axis parallel to prism axis), we would expect a rather diffuse (weak) texture pattern resulting in low texture indexes and weak {001} maxima. Indeed, near the surface of the shell, the individual second-order prisms are arranged in a spherical radiating pattern, that would decrease the texture strength (Fig. 4b). This is evidently not the case (see *Tectus niloticus* and *Tectus pyramis*) and we can conclude that the second-order prisms are morphologically similar but crystallographically non-equivalent. The crystallographic orientation is retained through non-repetitive morphological boundaries. Moreover, the parameters provided by both techniques (scanning electron microscopy and texture) could be taken into account in phylogenic discussions, since they are not redundant.

Mutvei (1978, 1980) observed striations formed by etching on nacre tablets and interpreted them as evidence for individual nacre tablets to be made of cyclic domains, related to each other by a {110} twin, giving rise to the pseudo-hexagonal symmetry of aragonite. Looking at the angles between Mutvei's striations, Hedegaard and Wenk (1998) suggested they may be crystallographically non-equivalent, time-synchronous growth sectors with different

Table 3
The main characteristics of nacre in the main molluscan clades. S and C stand for sheet and Columnar nacres respectively

	nacre	a axis	c axis
bivalves	S	*	⊥
cephalopods	C	*	⊥
gastropods	C	O	⊥
monoplacophoras	S	O	⊥

composition and solubility. None of the available information, including X-ray texture analysis, allows us to determine whether the individual tablets are single crystals (that may or may not be aligned in a twin-like pattern), a peculiar intergrowth of single twins (Mutvei, 1978, 1980), pseudo-hexagonal {110} trillings, or whether even Mutvei's sectors are mosaics of twinned domains and a detailed TEM study would be necessary to resolve this issue. Gastropod nacre is particularly troublesome, as the platelets are composed of a variable number of sectors in radiating aggregates, forming the platelets (Hedegaard, 1990), and the fibre texture is less oriented than that of other nacres. Swamy (1935) describes the nacres of *Pinctada vulgaris* and *Haliotis spp*. as single crystals, albeit in different orientation, emphasising a considerably smaller alignment in *Haliotis sp*. Swamy's data are unequivocal, but we can not verify them, as he did not indicate the species examined.

From our data it is clear that nacre textures differ between members of the major clades bivalves, cephalopods, gastropods, and monoplacophoras (Table 3). While all nacres exhibit perpendicular *c*-axes, double twin textures only appear in bivalves and cephalopods, fibre textures only in gastropods and cephalopods. Consequently, the crystallographic features of nacre tablets, e.g. of gastropods, differ from those of cephalopods (or bivalves versus monoplacophoras), which is not evident from scanning electron microscopy images. Furthermore, in bivalves, the twin volume fractions are impossible to determine by scanning electron microscopy, while texture analysis demonstrates considerable twin fractions.

Bøggild (1930) describes two orientations of optic axes in the second-order lamellae of simple crossed lamellar microstructures indicating that neighbouring lamellae are morphologically and crystallographically identical but rotated 180° relative to each other. Hedegaard and Wenk (1998) find the two *c*-axis maxima in the crossed lamellar layers of *Scutellastra tabularis* and *Fragum fragum* are inclined about 20–25° to the surface normal and (110) poles aligned perpendicular to the shell margin, corresponding to the two dip directions of the lamellae. This indicates that basal planes are parallel to the lamellae. It is reassuring to find two independent orientations in a shell structure with two main physical orientations of the shell microstructure observed by scanning electron microscopy. But we also find other textures (single crystal, single twin, double twin and fibre) in crossed lamellar layers, that are morphologically similar. This corresponds to our single twin pattern in *Oliva miniacea*, *Scutellastra tabularis* and *Fragum fragum*. Fig. 6 illustrates this for the inner radial and outer comarginal crossed lamellar layers of *Euglandina sp.*, both single crystal like (with a larger dispersion for the outer layer) where a split was expected because both are crossed layers, and as is seen with scanning electron microscopy. The lack of the pole splitting in {001} pole figures for crossed lamellae is even more evident in the case of the inner radial crossed lamellar layer of *Cyclophorus woodianus*. In this case (Fig. 10) successive lamellae are inclined at approximately 60° to each other, while the {001} pole maximum is one of the best localised, with a very high texture strength.

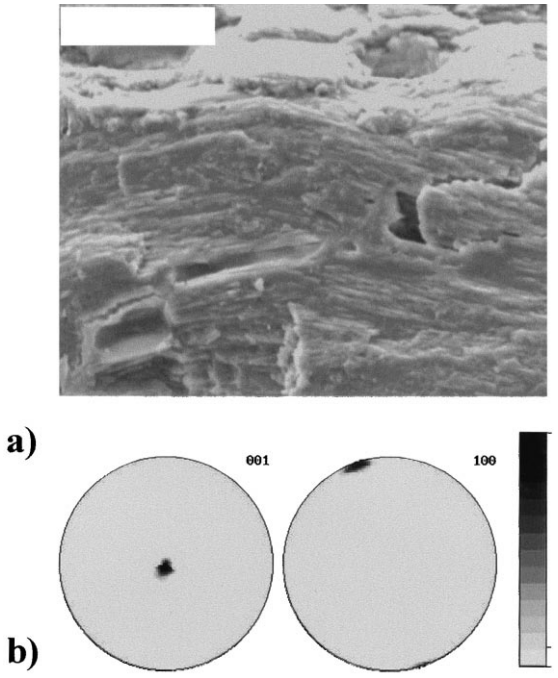

Fig. 10. (a) SEM backscattering image of the inner radial crossed lamellar layer of *Cyclophorus woodianus* (scale bar = 20 μm). (b) Corresponding {001} and {100} pole figures (max > 100 m.r.d., min = 0). Logarithmic density scale, equal area projection.

Wilmot et al. (1992) found that textures of the crossed lamellar layers of *Oliva sayana* and *Littorina littorea* differ from each other, but report that individual second-order lamellae are twinned in both. That is, the twinning pattern does not correspond to the dip directions of the second-order lamellae. Each lamella is profusely twinned on (1–10) (Wilmot et al. 1992).

The specimens of *Helix aspersa* have very thin shells with five distinct shell layers of, listing from outside to inside,

homogeneous (very thin), comarginal crossed lamellar, radial crossed lamellar, comarginal crossed lamellar and simple prismatic microstructure, of which the outer comarginal crossed lamellar layer is the thickest. Due to the thin shell and the X-ray beam penetration, several of these layers certainly contributed to the single crystal texture signal, and we conclude the layers are crystallographically aligned, even if morphologically different. Conversely, we found (Chateigner et al., 1996) different textures in neighbouring layers of very similar appearing comarginal, radial, and comarginal crossed lamellar microstructures in *Cypraea testudinaria*.

Irregular complex crossed lamellar layers emphasise the uncoupling of morphology and crystallography. Every irregular complex crossed lamellar layer has multiple morphological orientations of the lamellae, with distinct uniform crystallographic orientations (*Cellana testudinaria*, *Fissurella oriens* and *Nerita scabricosta*). Lamellae are morphologically similar but crystallographically non-equivalent. Bøggild (1930) describes the optic axes of complex crossed lamellar layers as varying between two extremes, equivalent to our dispersed *c*-axis pattern, which we do not observe in this microstructure type. Bøggild's description is obviously not valid for all complex crossed lamellar layers, but unquestionably for some.

Intersected crossed platy microstructure only occurs in vetigastropods (Hedegaard, 1990; Ponder and Lindberg, 1997), and all our samples have a fiber texture pattern with *c*-axis perpendicular to the shell (*Entemnotrochus adansonianus, Phasianella australis, Perotrochus quoyanus* and *Turbo petholatus*), as for nacres from vetigastropods, and we suspect the fibre texture with *c*-axis orthogonal to the shell surface is a typical vetigastropod character. We can not determine whether the platelets of intersected crossed platy microstructure are crystallographically equivalent and the fibre pattern is due to a partly random orientation of platelets, or whether the axes are differently oriented relative to the morphology of the platelets.

The homogenous microstructure is widely distributed in molluscs (Taylor et al., 1969, 1973; Hedegaard, 1990) and some of the simple prismatic microstructures observed in thin sections by Bøggild (1930) appear as 'homogeneous' when investigated by scanning electron microscopy (Hedegaard, 1990). Bøggild (1930), however, also describes a homogeneous microstructure, seemingly with a local orientation of optic axes, albeit variable over the range of a shell layer. This may correspond to our results for the outer homogeneous layer of *Cypraea testudinaria*. The important point is that homogeneous layers with little or no physical organisation from the scanning electron microscopy point of view (Carter and Clark, 1985), show distinct crystallographic orientations (see *Nautilus macromphalus, Cypraea testudinaria*), and even very strong textures (*Oliva miniacea*). Up to now we have seen only homogenous layers that are highly organised, not haphazard deposits of aragonite.

For differently represented clades, one can point out some tendencies. The sheet nacres from bivalves differ from that of monoplacophoras in their *a*-axis distribution, double twinned in the former while fibrous in the latter. The columnar nacre of cephalopods appears double twinned, while it is fibre textured in inside layers of gastropods.

Inside a family, we observe similar texture patterns for closely related taxa. For instance, bivalve nacres only exhibit double twins with perpendicular *c*-axes. But in bivalves, the twin fraction still varies and is regrouped around main values: very closely related species like *Bathymodiolus thermophilus* and *Mytilus edulis* show comparable twinned volumes, while more distant species exhibit quite different percentage of twins (e.g. *Pinctada sp.* versus *Mytilus sp.*).

Texture types are not identical for the same microstructural layer type, that scanning electron microscopy investigations cannot differentiate, and similar shell shape (the outer crossed lamellar layers of *Euglandina* and *Helix* species for instance), indicating a different *a*-axis alignment relative to the growth direction.

Finally, for one species and very similar layers (i.e. the crossed lamellae inside and outside *Viana regina*), there still exists a difference in the texture strength, the former layer exhibiting a larger texture index, pointing to a higher organisation.

7. Conclusions

This work points out that X-ray diffraction texture patterns may differ, even though the associated microstructures are similar. It shows that there is not a trivial relationship between these two complementary aspects of shell morphology. This may be explained by the strong interaction between the organic constituents that are controlling the growth (present at every step of the crystallisation of the shell) and the aragonite microstructure. Aragonite is a metastable phase of calcium carbonate under normal conditions, but is clearly stabilised in microstructures, which results in high mechanical strengths of the whole shells.

We conclude that there is not a simple one-to-one relationship between shell microstructures and crystallographic orientation, and neither is one merely a refinement of the other. Crystallography does not determine shell structure morphology, nor does shell structure morphology determine the crystallography. This means that both features add important, independent, and complementary characters for a phylogenetic discussion.

We have shown the wide variety of texture patterns and some systematic trends. In the future it will be interesting to apply these methods to fossil shells where aragonitic nacre has either been preserved or recrystallised, and to extend the study to calcite layers. While shells of living molluscs have not much relationship to structural geology, they nevertheless may become significant for studying the evolution of molluscs through geologic time with methods that are

routinely applied by structural geologists to investigate the deformation history of rocks.

Acknowledgements

We wish to thank the Museum of Palaeontology, University of California (Berkeley) USA for providing study material and facilities for C.H.; the United State National Museum of Natural History (Smithsonian Institution), for the specimens of *Entemnotrochus adansonianus* and *Perotrochus quoyanus* (USNM 878154); the Zoologisk Museum (Copenhagen) Denmark, for access to *Neopilina galatheae* (specimen V, Station 716); M. Laulier and F. Denis, Laboratoire de Biologie et Génétique Evolutive, Université du Maine (Le Mans) France and the MARVEL (1997) expedition for providing the specimen *Anodonta cygnea* and *Bathymodiolus thermophilus*; C.P. Meyer of University of California (Berkeley) kindly made *Cypraeidae* available from his research material. Barry Roth kindly identified the specimen of *Helminthoglypta nickliniana anachoreta*, straying into our sample material. We thank C. Porter, University of Guam; for making specimens available and some identifications.

The French Ministère de l'Education Nationale, de la Recherche et des Technologies, funded D.C.'s stay at University of California at Berkeley and two months at Université du Maine for C.H.. H.-R.W. is appreciative for support from the France-Berkeley Fund and the National Science Foundation. We acknowledge constructive reviews by K. Bandel (Hamburg) and J. Reitner (Göttingen).

References

Aizenberg, J., Ilan, M., Weiner, S., Addadi, L., 1996. Intracrystalline macromolecules are involved in the morphogenesis of calcite sponge spicules. Connective Tissue Research 34 (4), 255–261.

Aizenberg, J., Hanson, J., Koetzle, T.F., Weiner, S., Addadi, L., 1997. Control of macromolecule distribution within synthetic and biogenic single calcite crystals. Journal of the American Chemical Society 119, 881–886.

Batten, R.L., 1975. The Scissurellidae—Are they neotenously derived fissurellids? (Archaeogastropoda). American Museum Novitates 2567, 1–29.

Bobbio, A., 1972. The first endosseous alloplastic implant in the history of man. Bulletin of the Historical Dentology 20, 1–6.

Bøggild, O.B., 1930. The shell structure of the mollusks, Det Kongelige Danske Videnskabernes Selskabs Skrifter, Naturvidenskabelige og Mathematiske Afdeling, 9. R kke, II.2: 231–325, pl. I–XV.

Bunge (Ed.), H.-J., 1981. Textures in Materials Science. Butterworth, London.

Carter, J.G., 1980. Guide to bivalve shell microstructures. In: Rhoads, D.C., Lutz, R.A. (Eds.), Skeletal Growth of Aquatic Organisms. Plenum, New York.

Carter, J.G., 1990. Skeletal Biomineralisation: Patterns, Processes and Evolutionary Trends. Van Nostrand Reinhold, New York.

Carter, J.G., Clark II, G.R., 1985. Classification and phylogenetic significance of molluscan shell microstructure. In: Bottjer, D.J., Hickman, C.S., Ward, P.D., Broadhead, T.W. (Eds.), Molluscs, Notes for a Short Course. University of Tenessee, Department of Geological Sciences Studies in Geology, pp. 50–71.

Chateigner, D., Hedegaard, C., Wenk, H.-R., 1996. Texture analysis of a gastropod shell: *Cypraea testudinaria*. In: Liang, Z., Zuo, L., Chu, Y. (Eds.), Textures of Materials 2, pp. 1221–1226.

Chateigner, D., Hedegaard, C., Wenk, H.-R., 1999. Quantitative characterisation of mollusc shell textures. In: Szpunar, J.A. (Ed.), Textures of Materials, 2. NRC Research Press, Ottawa, Ontario, pp. 1495–1500.

Crick, R.E., 1989. Origin, Evolution, and Modern Aspects of Biomineralization in Plants and Animals. Plenum Press.

Falini, G., Albeck, S., Weiner, S., Addadi, L., 1996. Control of aragonite or calcite polymorphism by mollusk shell macromolecules. Science 271, 67–69.

Hedegaard, C., 1990. Shell Structures of the Recent Archaeogastropoda. PhD Thesis, University of Aarhus, Denmark, Vols. 1 and 2.

Hedegaard, C., 1997. Shell Structures of the recent Vetigastropoda. Journal of Molluscan Studies 63, 369–377.

Hedegaard, C., Wenk, H.-R., 1998. Microstructure and texture patterns of mollusc shells. Journal of Molluscan Studies 64, 133–136.

Heizmann, J.-J., Laruelle, C., 1986. Simultaneous measurement of several X-ray pole figures. Journal of Applied Crystallography 19, 467–472.

Kocks, U.F., Tomé, C., Wenk, H.-R., 1998. Texture and Anisotropy: Preferred Orientations in Polycrystals and Their Effect on Materials Properties. Cambridge University Press.

Lindberg, D.R., 1988. The patellogastropoda. Malacological Review, supplement 4, 35–63.

MacClintock, C., 1967. The shell structure of patelloid and bellerophontoid gastropods (Mollusca). Peabody Museum of Natural History. Yale University Bulletin 22, 1–140.

Mutvei, H., 1978. Ultrastructural characteristics of the nacre in some gastropods. Zoologica Scripta 7, 287–296.

Mutvei, H., 1980. The nacreous layer in molluscan shells. In: Omori, M., Watabe, N. (Eds.), The Mechanisms of Biomineralisation in Animals and Plants. Tokai University Press, pp. 49–56.

Ponder, W.F., Lindberg, D.R., 1997. Towards a phylogeny of gastropod molluscs: an analysis using morphological characters. Zoological Journal of the Linnean Society 119, 83–265.

Ricote, J., Chateigner, D., 1999. Quantitative texture analysis applied to the study of preferential orientations in ferroelectric thin films. Boletin de la Societad Española de Cerámica y Vidrio 38 (6), 587–591.

Ricote, J., Chateigner, D., Pardo, L., Algueró, M., Mendiola, J., Calzada, M.L., 2000. Quantitative analysis of preferential orientation components of ferroelectric thin films. Ferroelectrics 241, 167–174.

Runnegar, B., Pojeta Jr., J., Morris, N.J., Taylor, J.D., Taylor, M.E., Mcclung, G., 1975. Biology of the Hyolitha. Lethaia 8, 181–191.

Silve, C., Lopez, E., Vidal, B., Smith, D.C., Camprasse, S., Camprasse, G., Couly, G., 1992. Nacre initiates biomineralization by human osteoblasts maintained in vitro. Calcified Tissue International 51, 363–369.

Suga, N., 1991. Mechanisms and Phylogeny of Mineralization in Biological Systems. Springer Verlag.

Swamy, S., 1935. X-ray analysis of the structure of iridescent shells. Part II, The Haliotid. Proceedings of the Indian Academy of Sciences II (4), 345–351 pl. XVII–XVIII.

Taylor, J.D., Kennedy, W.J., Hall, A., 1969. The shell structure and mineralogy of the Bivalvia, introduction. *Nuculacea–Trigonacea*. Bulletin of the British Museum (Natural History), Zoology supplement 3, 1–125.

Taylor, J.D., Kennedy, W.J., Hall, A., 1973. The shell structure and mineralogy of the Bivalvia, Part II, *Lucinacea–Clavagellace*a. Bulletin of the British Museum (Natural History) Zoology 22 (9), 253–294.

Weiner, S., Addadi, L., 1997. Design strategies in mineralized biological materials. Journal of Materials Chemistry 7 (5), 689–702.

Weiner, S., Talmon, Y., Traub, W., 1983. Electron diffraction of mollusc shell organic matrices and their relationship to the mineral phase. International Journal of Biological Macromolecules 5, 325–328.

Weiner, S., Traub, W., 1980. X-ray diffraction study of the insoluble organic matrix of mollusk shells. FEBS letters 111, 311–316.

Weiner, S., Traub, W., 1981. Structural aspects of recognition and assembly. In: Balaban, M., Sussman, J.L., Traub, W., Yonath, A. (Eds.), Biological Macromolecules, Balaban ISS, Rehovot and Philadelphia, pp. 467–482.

Weiner, S., Traub, W., 1984. Macromolecules in mollusc shells and their functions in biomineralisation. Philosophical Transactions of the Royal Society, London Series B304, 425–434.

Wenk, H.-R., 1965. Eine photographische Roentgen-Gefuegeanalyse. Schweiz. mineral. petrog. Mitt. 45, 517–550.

Wenk, H.-R., Matthies, S., Donovan, J., Chateigner, D., 1998. BEARTEX: A Windows based program for quantitative texture analysis. Journal of Applied Crystallography 31, 262–269.

Wilmot, N.V., Barber, D.J., Taylor, J.D., Graham, A.L., 1992. Electron microscopy of molluscan crossed-lamellar microstructure. Philosophical Transactions of the Royal Society, London Series B337, 21–35.

Wise, S.W., 1970. Microarchitecture and mode of formation of nacre (mother-of-pearl) in Pelecypods, Gastropods, and Cephalopods. Eclogae Geologicae Helveticae 63, 775–797.